

Weakening of the Kuroshio Intrusion Into the South China Sea Under the Global Warming Hiatus

Chau-Ron Wu, You-Lin Wang, Yong-Fu Lin, Tzu-Ling Chiang, and Chao-Chi Wu

Abstract—We analyze a 22-year (1993–2014) record of the Kuroshio intrusion (KI) index defined from maps of mean absolute dynamic topography west of Luzon Island in the Philippines to investigate the long-term trend of the KI into the South China Sea (SCS). The monotonically increasing trend of the KI index extracted by empirical mode decomposition implies a slight decreasing trend of the meridional pressure gradient across the Luzon Strait, suggesting a weakening of the KI into the SCS based on the geostrophy. This weakening is largely due to an intensification of the upstream Kuroshio east of Luzon, which is closely correlated with the latitude of the North Equatorial Current (NEC) bifurcation off the Philippines. We also find that the latitude of the NEC bifurcation has tended to migrate southward in recent years, coincident with the strengthening of the Kuroshio east of Luzon. The forcing of the trends of low-latitude circulation is attributable to changing surface wind fields in the tropical Pacific. The trade winds have intensified in response to the recent global warming hiatus, and an anomalous cyclonic wind field has appeared over the Philippine Sea. Both of these phenomena have contributed to the southward migration of the NEC bifurcation latitude in recent years. This has led to enhance the Kuroshio transport east of Luzon, and the Kuroshio has tended to bypass the Luzon Strait without significant westward encroachment.

Index Terms—Climate change, Hiatus, Kuroshio intrusion, South China Sea.

I. INTRODUCTION

THE North Equatorial Current (NEC) bifurcates at around 12°N off the east coast of the Philippines (see Fig. 1). The northern branch forms the Kuroshio, which flows northward along the east coast of Luzon and Taiwan. Before reaching Taiwan, the Kuroshio either penetrates westward into the South China Sea (SCS) or bypasses the SCS, flowing northward in a relatively straight path across the Luzon Strait [1], [2], a gap in the western boundary approximately 350 km wide whose deepest channel reaches a depth of 2500 m. While water exchange mostly occurs through the Luzon Strait, the Kuroshio intrusion (KI) into the SCS significantly influences the mass, heat, salinity, and nutrient balances between the Pacific Ocean and SCS.

Intraseasonal, seasonal, and interannual variabilities of the Kuroshio meander east of Luzon Strait and Taiwan, and KI into

Manuscript received January 20, 2016; revised April 21, 2016; accepted May 25, 2016. Date of publication August 9, 2016; date of current version November 9, 2016. This work was supported by the Ministry of Science and Technology, ROC, under Grants MOST 104-2611-M-003-002-MY3 and 104-2811-M-003-018. This paper was subsidized by the National Taiwan Normal University, Taiwan. (Corresponding author: Chau-Ron Wu).

The authors are with the Department of Earth Sciences, National Taiwan Normal University, Taipei 116, Taiwan (e-mail: cwu@ntnu.edu.tw; ylwang@ntnu.edu.tw; yongfulin0711@gmail.com; tlchiangtw@gmail.com; gert83129@gmail.com).

Color versions of one or more of the figures in this paper are available online at <http://ieeexplore.ieee.org>.

Digital Object Identifier 10.1109/JSTARS.2016.2574941

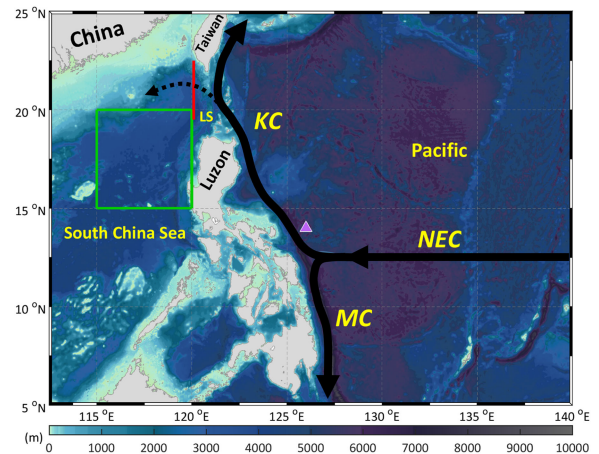


Fig. 1. Bathymetry of the study area. Solid arrows are the scheme of circulation pattern for the Kuroshio (KC), North Equatorial Current (NEC), and Mindanao Current (MC). Dotted arrow is the scheme of the Kuroshio intrusion (KI) into the South China Sea. Red line is the meridional section (19.5°N–22.5°N) of ~120°E denoting the western limit of the KI. Green rectangle is the domain (15°N–20°N, 115°E–120°E) serving as a sea level index for the KI into the South China Sea. The yellow “LS” and pink triangle denote the Luzon Strait and location of 14°N, 126°E, respectively.

the SCS have been reported from various observations [3]–[5] and model simulations [2], [6]. Both altimeter-based geostrophic current and modeled velocities indicate that the KI is mainly confined within a well-rounded Kuroshio meander in summer, but the water penetrates farther into the SCS, extending to 117°E during winter [6]. Wu and Hsin [6] further demonstrated that fluctuations in the regional wind field are closely related to the KI. An intense winter monsoon reinforces the upstream Kuroshio, enhancing the KI into the SCS. The seasonal cycle is a prominent fluctuation in the region, and is due to the seasonally reversing monsoon. There is also significant interannual variation. Most previous studies have attributed the interannual variation, which is observed in both the atmospheric and oceanic circulation, to the El Niño–Southern Oscillation (ENSO), which is known to have the largest impact on the interannual variability of the global climate, particularly in the tropical Pacific Ocean. However, a recent study by Wu [7] demonstrated that the interannual variability is strongly correlated with the Pacific Decadal Oscillation (PDO) [8] index, and not the ENSO, particularly in recent years. However, due to a lack of data, long-term phenomena and their variability have been less studied, and the effect of climate change on the KI on longer timescales remains poorly understood.

Both observations and model simulations have revealed that variation in the KI is closely related to its intensity off Luzon Island in the Philippines [9], [10]. For example, a numerical

simulation by Sheu *et al.* [10] demonstrated that when the Kuroshio transport at 18 °N decreases (increases), the KI into the SCS increases (decreases). Tracing patterns upstream, fluctuations in the Kuroshio transport east of Luzon, are associated with variation in the NEC bifurcation latitude off the Philippines [11], [12]. Toole *et al.* [11] observed that the transports of the NEC and the Kuroshio in spring 1988 were twice those in fall 1987. The increase in transport was accompanied by a marked southward shift of the NEC bifurcation latitude in 1988. Furthermore, variability in surface currents in the tropical Pacific is mainly induced by temporal variation in wind forcing. Fluctuating winds trigger a meridional shift in the NEC bifurcation latitude. Therefore, to elucidate variation in the surface ocean circulation, it is necessary to examine the climate conditions modulating the surface wind field in the tropical Pacific.

Since the late 1990s, there has been a decrease in the rate of global warming compared to that during the twentieth century despite continual increases in atmospheric greenhouse gases [13]. This decrease has been termed the “global warming hiatus.” During this hiatus, numerous pronounced changes in atmospheric circulation and surface winds have been observed globally, such as the strengthening of Pacific trade winds [14], [15], which suggests that the wind-driven circulation of the tropical Pacific responds/contributes to the hiatus [13]. Furthermore, the circulation of the tropical ocean, via the North Pacific subtropical gyre, impacts the Kuroshio. However, although it would be expected that variability in the Kuroshio should be closely correlated with the hiatus, it is difficult to elucidate in detail the ocean processes affecting the Kuroshio due to a lack of *in situ* observations and the impacts of the hiatus on the Kuroshio are poorly understood. We adopt an empirical mode decomposition (EMD) procedure to decompose satellite altimeter data into meaningful components of various amplitudes and frequencies. We focus on long-term trends that have been less studied in the region and examined the KI, upstream Kuroshio transport, meridional migration of the NEC bifurcation latitude, and wind forcing. We also investigate whether the surface wind field has varied with the PDO phase change under the recent global warming hiatus. Section II briefly describes the data and methodology used in this study. Section III shows the main results. Focusing on long-term trends, we use the EMD to extract a sea-level index for the KI for further interpretation. In addition, we investigate the possible causes of the long-term trend. Section IV examines the variability in the surface wind field and associated oceanographic responses under the hiatus. Section V summarizes the results.

II. DATA AND METHODOLOGY

Several satellite remote sensing datasets and model outputs have been used in this study. Altimeter-based sea surface height and geostrophic velocity data are distributed by Archiving, Validation, and Interpretation of Satellite Oceanographic data (AVISO; <http://www.aviso.altimetry.fr>) in the version of gridded global delayed-time maps of absolute dynamic topography and absolute geostrophic velocities, two-sat-merged (DT-MADT H and UV, two sat merged version). The version is merged from two missions in which are with the same ground

track along the available period, including TOPEX/Poseidon with ERS-1, TOPEX/Poseidon with ERS-2, Jason-1 with Envisat, Jason-2 with Envisat, Jason-2 with Cryosat-2, and Jason-2 with Saral/AltiKa. The product is available from January 1993 onward and has spatial and temporal resolutions of 1/4° and daily, respectively. AVISO data over waters shallower than 200 m are ignored and period of 1993–2014 is used in this study.

Blended wind product is provided by the National Oceanic and Atmospheric Administration/National Climate Data Center (NOAA/NCDC; <https://www.ncdc.noaa.gov/data-access/marineocean-data/blended-global/blended-sea-winds/>). This product has blended multiple satellites, such as SSM/I, TMI, QuikSCAT, and AMSR-E, and is with temporal resolution of monthly and spatial resolution of 1/4° [16]. Additional four wind products used include National Centers for Environmental Prediction/National Center for Atmospheric Research (NCEP/NCAR) Reanalysis (NCEP1; <http://www.esrl.noaa.gov/psd/data/gridded/data.ncep.reanalysis.html> [17] provided by NOAA/NCEP/Climate Prediction Center (NOAA/NCEP/CPC), NCEP-Department of Energy Atmospheric Model Intercomparison Project II (NCEP-DOE AMIP-II) Reanalysis (NCEP2; <http://www.esrl.noaa.gov/psd/data/gridded/data.ncep.reanalysis2.html> [18] provided by NOAA/NCEP/CPC, Japanese 55-year Reanalysis (JRA-55; <http://jra.kishou.go.jp/JRA-55>) [19] provided by Japan Meteorological Agency (JMA), and European Center for Medium-Range Weather Forecasts (ECMWF) reanalysis-Interim (ERA-Interim) [20] provided by ECMWF (<http://www.ecmwf.int/en/research/climate-reanalysis/era-interim/>). All wind data are converted to monthly mean after downloaded.

Satellite-tracked surface drifting buoys from NOAA/Atlantic Oceanographic and Meteorological Laboratory/Global Drifter Program (NOAA/AOML/GDP; <http://www.aoml.noaa.gov/phod/dac/index.php>) are also obtained for this study. The drifter data provide sea surface velocity Lagrangian measurements (near 15 m depth) via Argos satellite-based system tracking, with temporal resolution of 6-hourly [21]. Drifter data are prepared for gridded mean with spatial and temporal resolutions of 1/2° and monthly, respectively. Additional velocity data are adopted from four products, including Hybrid Coordinate Ocean Model (HYCOM; <http://hycom.org/>) [22] provided by Global Ocean Data Assimilation Experiment/National Ocean Partnership Program (GODAE/NOPP), Japan Coastal Ocean Predictability Experiment 2 (JCOPE2; <http://www.jamstec.go.jp/frcgc/jcope/>) [23] provided by the Japan Agency for Marine-Earth Science and Technology (JAMSTEC), Global Ocean Data Assimilation System (GODAS; <http://www.cpc.ncep.noaa.gov/products/GODAS/>) [24] provided by NOAA/NCEP/CPC, and Ocean Reanalysis System 4 (ORAS4; <http://www.ecmwf.int/en/research/climate-reanalysis/ocean-reanalysis/>) [25] provided by ECMWF. All modeled velocity data (near 15 m depth) are converted to monthly mean after downloaded. The monthly indices of PDO and Niño 3.4 are provided by the Joint Institute for the Study of the Atmosphere and Ocean (JISAO; <http://research.jisao.washington.edu/pdo/>) and NOAA/NCEP/CPC (<http://www.cpc.ncep.noaa.gov/data/indices/>), respectively.

The conventional empirical orthogonal function (EOF), a linear method, is unsuitable to analyze the KI because each EOF mode represents only one portion of the source data and the corresponding time series is not required for a specified frequency. The EMD method is used to decompose a long-term continuous time series dataset into a finite number of components, the so-called “intrinsic mode functions” (IMFs) and residue (mean trend). The EMD is adaptive and consists of independent IMFs, each of which has an orthogonal amplitude and frequency. An IMF is defined as a function that possesses the same number of extrema and zero crossings. It also has a symmetric upper/lower envelope defined by the local maxima/minima. The sifting process finally stops when the residue becomes a monotonic function from which no more IMFs can be extracted. Due to the dyadic filter bank of the EMD algorithm, in practice, the number of IMFs modes is generally less than $\log_2(N)$, where N is the length of the dataset [26], [27]. For interpretation of temporally changing phenomena, the IMFs are more physically meaningful than the EOF modes. The EMD method is particularly useful for nonstationary and nonlinear time series, and has been used in various geophysical studies [28]–[30].

III. RESULTS

A. Trends in the KI

Wu [7] demonstrated that the KI into the SCS is closely correlated with the low sea level west of Luzon Island, the Philippines, and defined a sea level index to indicate KI variability. The defined KI index (sea level averaged over the domain of 15°N – 20°N and 115°E – 120°E , green rectangle in Fig. 1) serves as a good indicator for variability in the intrusion [7]. We perform the EMD on 22-year daily DT-MADT H in the area of the KI (top panel in Fig. 2) to obtain the instantaneous frequency. The EMD yielded eight IMFs and residue (see Fig. 2). The 1st to 4th IMFs are short-period fluctuations below the seasonal timescale. The fifth IMF contains a strong annual signal. While 6th to 8th IMFs show interannual and decadal variabilities of various amplitudes, the residue defines the tendency and is the focus of this study.

The residue shows a prominent long term increase of >16 cm from 1993 to 2014 (see Fig. 2). The monotonically increasing trend of the DT-MADT H suggests a weakening of the KI. The meridional sea level difference west of the Luzon Strait, which is lower to the south, is often a reliable proxy for the intensity of the KI into the SCS. Based on the geostrophy, the KI branch weakens if the difference in the meridional sea level decreases. To a certain degree, the KI index indicates the southern sea-level component (northwest of Luzon), and the increasing trend results in a weaker meridional pressure gradient which is associated with weakening of the KI into the SCS.

In general, the Kuroshio makes a larger meander, and penetrates westward into the SCS in winter, but tends to bypass the Luzon Strait in summer. Focusing on the winter intrusion and confirming the trend of the intrusion, we plot time series of the AVISO zonal altimeter-based geostrophic velocity anomaly along $\sim 120^\circ\text{E}$ (red line in Fig. 1) in the winters of 1993–2014

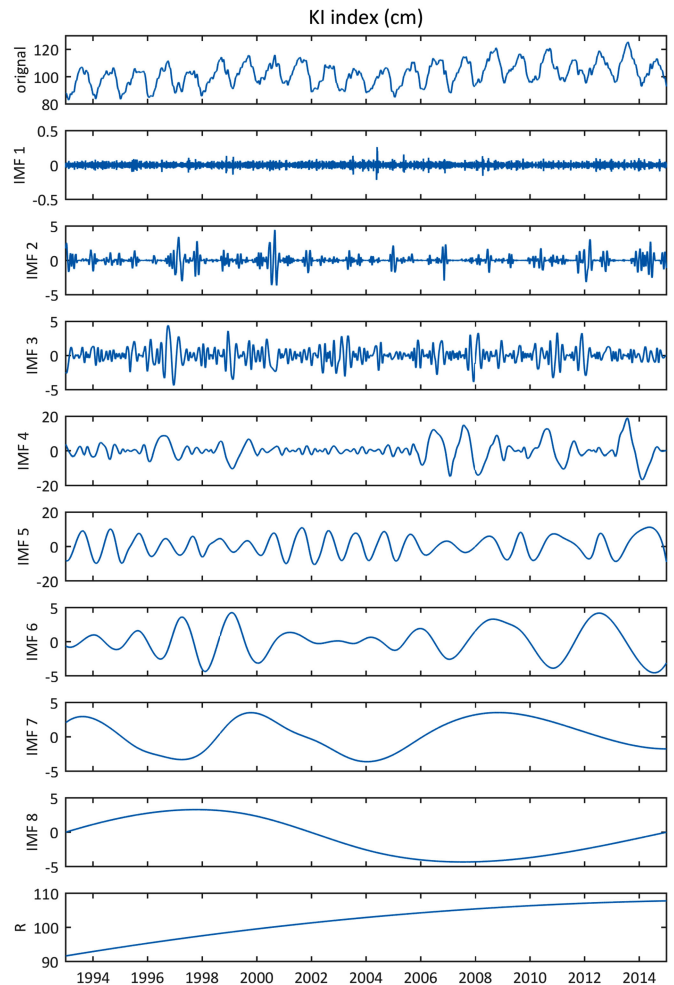


Fig. 2. Time series of 22-year daily KI index (AVISO DT-MADT H averaged over the domain of green rectangle in Fig. 1) and its EMD components. There are eight Intrinsic Mode Functions (IMFs) and residue (R). AVISO data over waters shallower than 200 m are not used.

(see Fig. 3). The selection of the longitude 120°E follows Wu and Hsin [6] who reported that this longitude can serve as an appropriate index for the definition of the westward KI based on both model outputs and AVISO geostrophic velocity maps. The 22-year satellite-based geostrophic velocity dataset along the meridional section of $\sim 120^\circ\text{E}$ reveals an intensified westward velocity visible only during wintertime and significantly weakened in the other seasons (figure not shown), which is in agreement with previous findings. Applying a linear fit from 1993 to 2014, the winter westward velocity decreased by $5 \text{ mm s}^{-1} \text{ yr}^{-1}$, indicating a weakening KI during the period (see Fig. 3). This decreasing tendency lends further support to the trend observed in the EMD.

In addition, the KI into the SCS likely depends on the strength of the upstream Kuroshio off Luzon Island in the Philippines [13]. Based on a correlation map between the KI index and the western North Pacific, Wu [7] reported that the KI index is closely correlated with the velocity core of the westward-flowing NEC and northward-flowing Kuroshio along the east

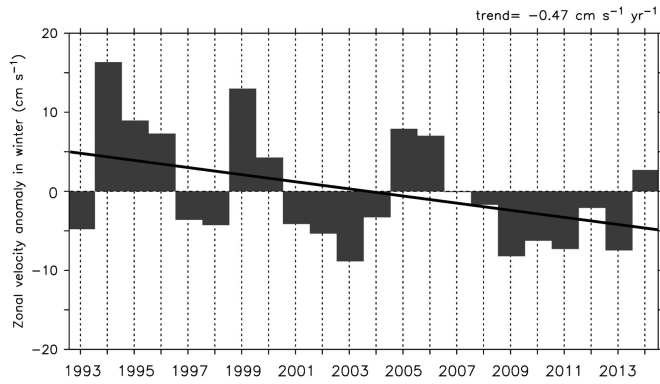


Fig. 3. Time series of AVISO DT-MADT zonal absolute geostrophic velocity (U) anomaly averaged over the section of red line in Fig. 1 in the winters of 1993–2014. Positive value represents westward flow. All time series are obtained by averaging original daily time series year by year over the episode from December to February of the following year. Bold black line indicates the linear trend and it is significant at the 95% confidence level. AVISO data over waters shallower than 200 m are not used.

coast of the Philippines ([7, Fig. 3]). The correlation map confirms that the fluctuations in the intrusion could be tracked back to the variation in the upstream Kuroshio east of Luzon, as well as the NEC variability in the equatorial Pacific Ocean.

Next, we use Argos satellite-tracked drifters that provide instantaneous velocity measurements of surface current to calculate the trends in the upstream KI. Negative trends dominate over the western North Pacific Ocean during 1993–2014, except for one localized anomaly (in red) northeast of Luzon Island [see Fig. 4(a)], indicating that the upstream Kuroshio east of Luzon increases in intensity from 1993 to 2014. Other datasets also reveal a similar pattern. The independent datasets of the satellite-derived geostrophic velocities (AVISO) and four ocean reanalysis products near 15 m depth (HYCOM, JCOPE2, GODAS, and ORAS4), each of which is subjected to the distinct assimilation method or simulation setting, consistently display an intensification of the upstream Kuroshio east of Luzon, although of different magnitudes [see Fig. 4(b)–(f)]. Estimates from linear fits of all of the independent datasets averaged over all acceleration areas inside the red rectangle shown in Fig. 4 from 1993 to 2014 reveal an enhanced Kuroshio east of Luzon [see Fig. 4(g)]. Increased Kuroshio transport produces greater inertia, which enables the Kuroshio to flow northward in a relatively straight path from east of Luzon to east of Taiwan. With weaker transport, the Kuroshio would tend to penetrate westward into the SCS. Such behavior of western boundary currents and their dependence on the inertia are well illustrated in a reduced-gravity model [31], and confirmed in a laboratory study of the phenomenon [32].

B. Trends in the NEC Bifurcation Latitude and Their Causes

Tracing back to the source region of the Kuroshio shows that the Kuroshio's strength east of Luzon is largely related to the NEC bifurcation latitude off the Philippines. Hydrographic surveys off the Philippine coast lend further support to this correlation. For example, Toole *et al.* [11] observed that the

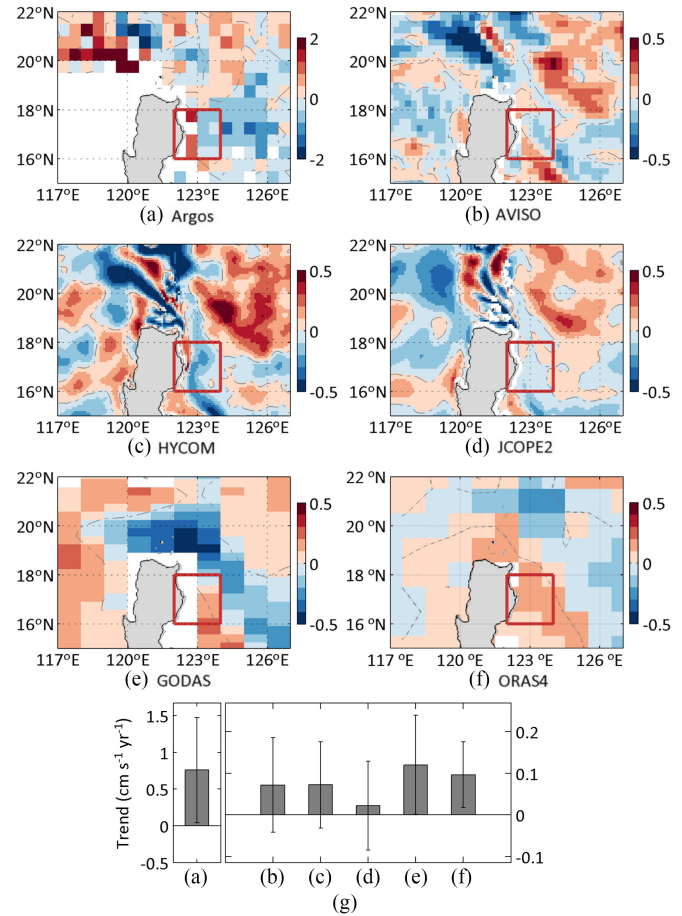


Fig. 4. Linear trend (unit in $\text{cm s}^{-1} \text{yr}^{-1}$) of monthly upstream Kuroshio intensity from (a) Argos, (b) AVISO, (c) HYCOM, (d) JCOPE2, (e) GODAS, and (f) ORAS4 during 1993–2014. In (a) and (b), trends are derived while data covers at least 12 years from 1993 to 2014 (22 years) and with depths more than 200 m, respectively. Red rectangle indicates the upstream region of the Kuroshio (15°N – 18°N , 122°E – 124°E), which is used to calculate the trend of upstream Kuroshio intensity in (g). Error bars indicate the 90% confidence interval.

transports of the Kuroshio in spring 1988 were twice those in fall 1987. Accompanying this increase in the transport was a marked southward shift of the NEC bifurcation latitude in 1988 [11].

We use five datasets to calculate the linear trend in the annual NEC bifurcation latitude, including the satellite-derived geostrophic components, as well as the GODAS, ORAS4, JCOPE2, and HYCOM reanalysis products. Fig. 5(a) shows the five time series of annual NEC bifurcation latitude from 1993 to 2014. The time series estimated from the AVISO altimeter data [red curve in Fig. 5(a)] has the largest variability of all five time series, migrating significantly from around 16°N to 11°N during the strongest El Niño event during 1997/1998. Fluctuations of similar phase are evident in all four reanalysis products. In the interannual and longer term variability, it can be observed that changes in the NEC migration are more closely correlated with the PDO than ENSO during 1993–2014 [see Fig. 5(b)], which is in agreement with Wu [7].

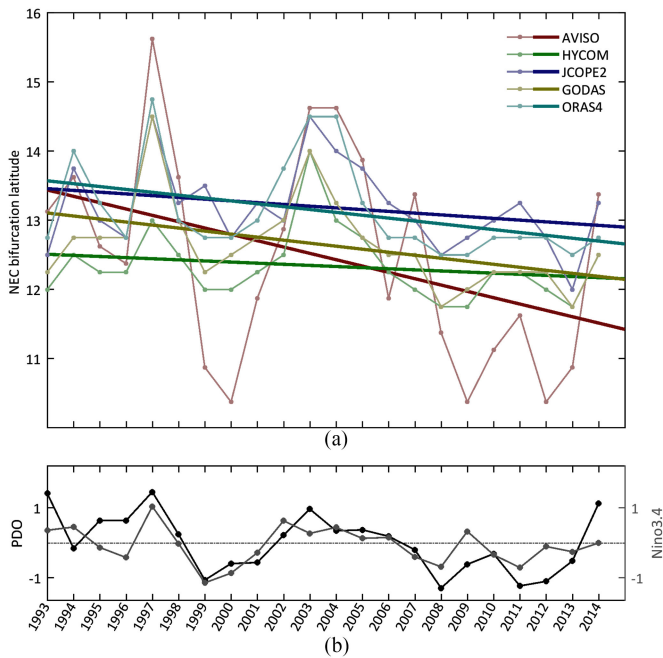


Fig. 5. Time series of annual (a) NEC bifurcation latitude based on AVISO, HYCOM, JCOPE2, GODAS, and ORAS4 products and (b) PDO and Niño 3.4 indices during 1993–2014. Linear trends of (a) are -0.09 , -0.02 , -0.03 , -0.04 , and -0.04 (degree yr^{-1}), respectively. Linear trends from AVISO, GODAS, and ORAS4 are significant at the 90% confidence level, while HYCOM and JCOPE2 are not significant. All data over waters shallower than 200 m are not used.

In addition, a linear fit of the annual NEC bifurcation latitude shows a prominent long-term trend, and the bifurcation has progressively shifted south over the past 22 years. This is consistently shown by all five datasets. The NEC bifurcation latitude inferred from AVISO altimeters (red bold line) migrates southward at a mean rate of 0.09° latitude per year. Although the rates are lower, all four reanalysis products also indicate a southward migration of the NEC bifurcation latitude during 1993–2014 with varying magnitudes (see Fig. 5). The southward migration of the NEC bifurcation latitude results in a larger Kuroshio east of Luzon, causing the Kuroshio to flow northward in a relatively straight path from east of Luzon to east of Taiwan. This southward trend is related to low-latitude climate conditions and needs to be further specified.

It is thought that the meridional shift in the NEC bifurcation latitude is triggered by wind fluctuations in the low-latitude North Pacific Ocean [12], [33]. Based on satellite altimeter measurements, Qiu and Chen [33] reported positive trends in zonal transport in the 2°N – 5°N and 13°N – 20°N bands and negative trends in the 5°N – 13°N band in the 1993–2009 period. They further demonstrated that regional sea level and circulation trends detected in the western tropical Pacific Ocean are closely correlated with the dynamic response to the changing surface wind stress field, and the appearance of these alternating bands reflects the combined effects of the southward migration of the tropical gyre.

The linear trends of winds in the Pacific basin from five wind products (NOAA/NCDC blended wind, NCEPr1, NCEPr2, JRA-55, and ERAint) are shown in Fig. 6. All five datasets

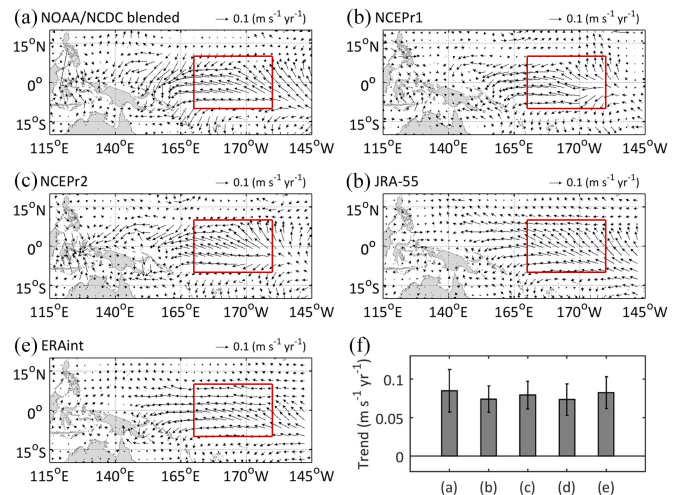


Fig. 6. Linear trend (unit in $\text{m s}^{-1} \text{yr}^{-1}$) of the monthly Pacific basin wind from various wind products from (a) NOAA/NCDC blended, (b) NCEPr1, (c) NCEPr2, (d) JRA-55, and (e) ERAint [(a): 1993–2010; (b)–(e): 1993–2014]. Red rectangle (10°S – 10°N , 170°E – 200°E) is used to calculate the trade wind tendency in (f). Error bars indicate the 90% confidence interval.

show intensified trade winds during 1993–2014. The strengthening trade winds induce a broad-scale negative Ekman flux divergence in the tropical North Pacific Ocean, which causes the southward migration of the tropical gyre, and, consequently, the southward migration of the NEC. The wind patterns and associated oceanographic response are consistent with another recent study [33]. Using a $1\frac{1}{2}$ -layer reduced-gravity model forced by the ECMWF reanalysis wind stress data, Qiu and Chen [33] demonstrated that the NEC's southward migration and strengthening can be attributed to the enhanced easterly trade winds across the tropical Pacific Ocean.

IV. DISCUSSION

Numerous pronounced changes in atmospheric circulation and surface winds have been observed globally during the global warming hiatus. Surface wind anomalies in the North Pacific in turn modulate the circulation of the western boundary currents. Furthermore, wind patterns in the Pacific with weakened westerlies, intensified trade winds, and wind stress curl under the warming hiatus are very similar to those in the negative PDO phase (figure not shown), implying that the hiatus may have been closely correlated with the PDO regime shift from positive to negative since the mid-1990s, which coincides with the hiatus [13].

We examine the climate conditions in the low-latitude western North Pacific Ocean during 1993–2014 and focus on the cold PDO phase because of its significant impact on the region, particularly in recent years. Fig. 7 shows the regional wind stress anomaly curl composite for the cold PDO phase. The composite is generated over the episodes when the negative PDO index is less than one standard deviation. An apparent positive wind stress curl centered at $\sim 14^\circ\text{N}$, 126°E (plotted in Fig. 1) is visible over the Philippine Sea. The variation in wind stress curl produces an anomalous cyclonic wind field, and the anomalous

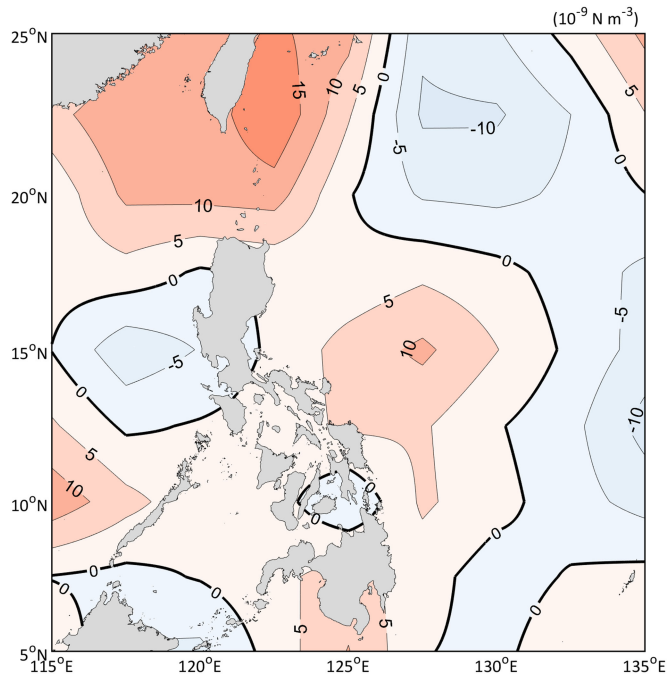


Fig. 7. Wind stress anomaly curl composite for the cold PDO phase based on the NCEPv1 product during 1993–2014. The composite is performed over the episodes when the negative PDO index is less than one standard deviation. Contour interval is $5 \times 10^{-9} \text{ N}\cdot\text{m}^{-3}$.

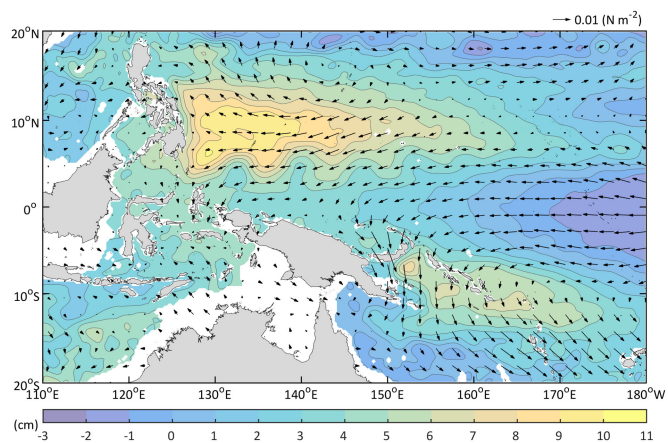


Fig. 8. Same as Fig. 7, but for NCEPv1 wind stress anomaly (vectors) together with AVISO DT-MADT H anomaly (shading). AVISO data over waters shallower than 200 m are not shown.

northerly wind off the Philippines induces a southward shift of the NEC bifurcation latitude during the cold PDO phase. The southward migration of the NEC leads to an enhanced Kuroshio transport east of Luzon, and in recent years, the Kuroshio has tended to bypass the Luzon Strait without significant westward encroachment.

In addition to the variation in wind stress curl off the Philippines, the intensified trade winds also contribute to the southward migration of the NEC bifurcation latitude. Fig. 8 shows the wind stress anomaly and sea surface height anomaly composite

for the cold PDO phase during 1993–2014. The composite is also generated over the episodes when the negative PDO index is less than one standard deviation. A strengthening of the trade winds is shown in the western tropical Pacific Ocean, which can be attributed to the global warming hiatus. The associated trends in sea level rise in the low-latitude western North Pacific Ocean are largely attributable to a redistribution of the upper ocean water mass caused by the stronger trade winds. Both the NEC bifurcation latitude and the tropical gyre are expected to migrate equatorward in response to the intensified trade winds.

V. SUMMARY

We conclude a decreasing trend in the KI into the SCS under the recent global warming hiatus. Trade winds in the tropical North Pacific have strengthened their intensity under the hiatus. The intensified trade winds have induced a broad-scale negative Ekman flux divergence, which causes a southward migration of the NEC. While an enhanced Kuroshio transport east of Luzon is usually associated with a southward shift in the NEC, the Kuroshio tends to flow northward in a relatively straight path and bypass the Luzon Strait without extensive westward intrusion because of stronger inertia.

The PDO regime shift from positive to negative since the mid-1990s coincides with the global warming hiatus. Our study demonstrates that an anomalous cyclonic wind field produced by variation in the wind stress curl appears over the Philippine Sea during the cold PDO phase. A dynamic response with the intensified trade winds and anomalous northerly winds off the Philippines also induce a southward shift of the NEC bifurcation latitude and the sequential intensification of the Kuroshio east of Luzon, resulting in weakening of the KI into the SCS.

REFERENCES

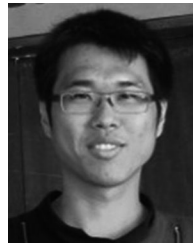
- [1] P.-T. Shaw, “The seasonal variation of the intrusion of the Philippine sea water into the South China Sea,” *J. Geophys. Res.*, vol. 96, no. C1, pp. 821–827, Jan. 1991.
- [2] C.-R. Wu and T.-L. Chiang, “Mesoscale eddies in the northern South China Sea,” *Deep Sea Res., Part II*, vol. 54, no. 14–15 pp. 1575–1588, Jul. 2007.
- [3] A. Farris and M. Wimbush, “Wind-induced Kuroshio intrusion into the South China Sea,” *J. Oceanogr.*, vol. 52, no. 6, pp. 771–784, Nov. 1996.
- [4] I.-F. Tsui and C.-R. Wu, “Variability analysis of Kuroshio intrusion through Luzon Strait using growing hierarchical self-organizing map,” *Ocean Dyn.*, vol. 118, no. 8, pp. 1170–1181, Aug. 2013.
- [5] P. C. Hsu, C. C. Lin, S.-J. Huang, and C.-R. Ho, “Effects of cold eddy on Kuroshio meander and its surface properties, east of Taiwan,” *IEEE J. Sel. Topics Appl. Earth Observ. Remote Sens.*, 2016, to be published.
- [6] C.-R. Wu and Y.-C. Hsin, “The forcing mechanism leading to the Kuroshio intrusion into the South China Sea,” *J. Geophys. Res.*, vol. 117, no. C7, pp. C07015, Jul. 2012.
- [7] C.-R. Wu, “Interannual modulation of the Pacific Decadal Oscillation (PDO) on the low-latitude western North Pacific,” *Prog. Oceanogr.*, vol. 110, pp. 49–58, Mar. 2013.
- [8] N. J. Mantua, S. R. Hare, Y. Zhang, J. M. Wallace, and R. C. Francis, “A Pacific interdecadal climate oscillation with impacts on Salmon production,” *Bull. Amer. Meteorol. Soc.*, vol. 78, no. 6, pp. 1069–1079, Jun. 1997.
- [9] T. Qu and R. Lukas, “The bifurcation of the north equatorial current in the Pacific,” *J. Phys. Oceanogr.*, vol. 33, no. 1, pp. 5–18, Jan. 2003.
- [10] W.-J. Sheu, C.-R. Wu, and L.-Y. Oey, “Blocking and westward passage of eddies in the Luzon Strait,” *Deep Sea Res., Part II*, vol. 57, no. 19–20, pp. 1783–1791, 2010.

- [11] J. K. Toole, R. C. Millard, Z. Wang, and S. Pu, "Observations of the Pacific North Equatorial Current bifurcation at the Philippine coast," *J. Phys. Oceanogr.*, vol. 20, no. 2, pp. 307–318, Feb. 1990.
- [12] B. Qiu and S. Chen, "Interannual-to-decadal variability in the bifurcation of the North Equatorial Current off the Philippines," *J. Phys. Oceanogr.*, vol. 40, no. 11, pp. 2525–2538, Nov. 2010.
- [13] M. H. England *et al.*, "Recent intensification of wind-driven circulation in the Pacific and the ongoing warming hiatus," *Nature Clim. Change*, vol. 4, no. 3, pp. 222–227, Mar. 2014.
- [14] Y. Kosaka and S.-P. Xie, "Recent global-warming hiatus tied to equatorial Pacific surface cooling," *Nature*, vol. 501, no. 7467, pp. 403–407, Sep. 2013.
- [15] K. E. Trenberth, J. T. Fasullo, G. Branstator, and A. S. Phillips, "Seasonal aspects of the recent pause in surface warming," *Nature Clim. Change*, vol. 4, no. 10, pp. 911–916, Oct. 2014.
- [16] H. M. Zhang, J. J. Bates, and R. W. Reynolds, "Assessment of composite global sampling: Sea surface wind speed," *Geophys. Res. Lett.*, vol. 33, no. 17, pp. L17714, Sep. 2006.
- [17] E. Kalnay *et al.*, "The NCEP/NCAR 40-year reanalysis project," *Bull. Amer. Meteorol. Soc.*, vol. 77, no. 3, pp. 437–471, Mar. 1996.
- [18] M. Kanamitsu *et al.*, "NCEP-DOE AMIP-II reanalysis (R-2)," *Bull. Amer. Meteorol. Soc.*, vol. 83, no. 11, pp. 1631–1643, Nov. 2002.
- [19] S. Kobayashi *et al.*, "The JRA-55 reanalysis: General specifications and basic characteristics," *J. Meteorol. Soc. Jpn.*, vol. 93, no. 1, pp. 5–48, Feb. 2015.
- [20] D. P. Dee *et al.*, "The ERA-Interim reanalysis: Configuration and performance of the data assimilation system," *Quart. J. Roy. Meteorol. Soc.*, vol. 137, no. 656, pp. 553–597, Apr. 2011.
- [21] R. Lumpkin and M. Pazos, "Measuring surface currents with surface velocity program drifters: The instrument, its data and some recent results," in *Lagrangian Analysis and Prediction of Coastal and Ocean Dynamics*, A. Griffa *et al.*, Ed. Cambridge, U.K.: Cambridge Univ. Press, 2007, pp. 39–67.
- [22] R. Bleck and D. B. Boudra, "Initial testing of a numerical ocean circulation model using a hybrid (quasi-isopycnic) vertical," *J. Phys. Oceanogr.*, vol. 11, no. 6, pp. 755–770, Jun. 1981.
- [23] Y. Miyazawa *et al.*, "Water mass variability in the western North Pacific detected in a 15-year eddy resolving ocean reanalysis," *J. Oceanogr.*, vol. 65, no. 6, pp. 737–756, Dec. 2009.
- [24] J. Derber and A. Rosati, "A global oceanic data assimilation system," *J. Phys. Oceanogr.*, vol. 19, no. 9, pp. 1333–1347, Sep. 1989.
- [25] M. A. Balmaseda, K. Mogensen, and A. T. Weaver, "Evaluation of the ECMWF ocean reanalysis system ORAS4," *Quart. J. Roy. Meteorol. Soc.*, vol. 139, no. 674, pp. 1132–1161, Jul. 2013.
- [26] N. E. Huang *et al.*, "The empirical mode decomposition and the Hilbert spectrum for nonlinear and non-stationary time series analysis," *Proc. R. Soc. Lond. A*, vol. 454, no. 1971, pp. 903–995, Mar. 1998.
- [27] N. E. Huang and Z. Wu, "A review on Hilbert-Huang transform: Method and its applications to geophysical studies," *Rev. Geophys.*, vol. 46, no. 2, pp. RG2006, Jun. 2008.
- [28] T. Ezer, W. D. Heyman, C. Houser, and B. Kjerfve, "Modeling and observations of high-frequency flow variability and internal waves at a Caribbean reef spawning aggregation site," *Ocean Dyn.*, vol. 61, no. 5, pp. 581–598, May 2011.
- [29] T. Udelhoven, "TimeStats: A software tool for the retrieval of temporal patterns from global satellite archives," *IEEE J. Sel. Topics Appl. Earth Observ. Remote Sens.*, vol. 4, no. 2, pp. 310–317, Jun. 2011.
- [30] T. Ezer, "Sea level rise, spatially uneven and temporally unsteady: Why the U.S. East Coast, the global tide gauge record, and the global altimeter data show different trends," *Geophys. Res. Lett.*, vol. 40, no. 20, pp. 5439–5444, Oct. 2013.
- [31] V. A. Sheremet, "Hysteresis of a western boundary current leaping across a gap," *J. Phys. Oceanogr.*, vol. 31, no. 5, pp. 1247–1259, May 2001.
- [32] V. A. Sheremet and J. Kuehl, "Gap-leaping western boundary current in a circular tank model," *J. Phys. Oceanogr.*, vol. 37, no. 6, pp. 1488–1495, Jun. 2007.
- [33] B. Qiu and S. Chen, "Multidecadal sea level and gyre circulation variability in the Northwestern Tropical Pacific Ocean," *J. Phys. Oceanogr.*, vol. 42, no. 1, pp. 193–206, Jan. 2012.



Chau-Ron Wu received the Ph.D. degree in physical oceanography from North Carolina State University, Raleigh, NC, USA, in 1998.

He is currently the Vice President for Research and Development with National Taiwan Normal University, Taipei, Taiwan. His research interests include ocean dynamics, numerical modeling, satellite oceanography, atmosphere-ocean processes, and climate variability.



You-Lin Wang received the B.S. degree in life science from Chinese Culture University, Taipei, Taiwan, in 2008. He is currently working toward the Ph.D. degree with the Department of Earth Sciences, National Normal Taiwan University, Taipei.

His research interests include climate change, western boundary current dynamics, and ocean-atmosphere interaction.



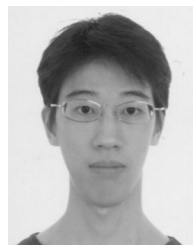
Yong-Fu Lin received the B.S. degree in marine environmental engineering from National Kaohsiung Marine University, Kaohsiung, Taiwan, in 2010, and the M.S. degree in marine environmental science and technology from National Taiwan Normal University, Taipei, Taiwan, in 2013, where he is currently working toward the Ph.D. degree with the Department of Earth Sciences.

His research interests include satellite remote sensing data analysis of oceanographic phenomena, climate change, and biogeographic distribution.



Tzu-Ling Chiang received the Ph.D. degree in earth sciences from National Taiwan Normal University, Taipei, Taiwan, in 2010.

She is currently a Postdoctoral Research Fellow with the Department of Earth Sciences, National Taiwan Normal University. Her research interests include ocean dynamics, numerical ocean circulation modeling, and satellite remote sensing.



Chao-Chi Wu received the B.S. and M.S. degrees in oceanography from National Taiwan Ocean University, Keelung, Taiwan, in 2006 and 2008, respectively.

He is currently a Research Associate with the Physical Oceanographic Laboratory, National Taiwan Normal University, Taipei, Taiwan. His research interests include image processing, satellite remote sensing data analysis, and numerical ocean model application.